JOURNAL OF PROPULSION AND POWER
Vol. 15, No. 4, July–August 1999

Simulation of Unsteady Flow in Nozzle-Ejector Mixer

Thomas Z. Dong* and Reda R. Mankbadi†
NASA John H. Glenn Research Center at Lewis Field, Cleveland, Ohio 44135

A numerical-simulation capability is developed with emphasis on capturing the flow and acoustic disturbances in internal flows. The configuration considered is that of a circular ejector with single-element primary nozzle. The Favre-filtered Navier–Stokes equations with a subgrid model are used to simulate the large-scale structure. The high-order dispersion-relation-preserving scheme is used to minimize dispersion and dissipation errors. Special boundary treatments are adopted for inflow, outflow, and solid walls to eliminate nonphysical reflections. Results show the growth of the disturbances, the formation of weak shock-cell structures, and the propagation of acoustic waves.

I. Introduction

THE mixer/ejector nozzle is a relatively new and promising concept for jet noise reduction. Its basic idea is to mix a large amount of ambient air with the flow from the engine's core exhaust to reduce the jet velocity and the associated noise. A schematic sketch is given in Fig. 1. Several mixer/ejector configurations have been developed and studied in the past.[1–4] The unsteady field inside the ejector mixer influences the jet noise in several ways. First, it directly radiates sound to the far field through the openings. Second, the unsteady flow dynamics inside the ejector/mixer determine the exit unsteady flowfield. The latter is actually the unsteady inflow to the jet plume, which determines its development in the initial region and the far-field radiated sound.

The Reynolds-averaged Navier–Stokes (RANS) equations can describe the mean flow inside the ejector mixer, but not the unsteady flowfield. The full, time-dependent, compressible Navier–Stokes equations govern the generation of sound and its propagation. In theory, direct numerical simulations (DNSs) based on these equations provide both the flow fluctuations and the acoustic field. However, the resolution requirement for high-Reynolds-number turbulent flows makes DNS impractical because of current computer limitations. As such, it was proposed in Refs. 5–7 to use large-eddy simulations (LESs) in computational aeroacoustics. In LES, the full Navier–Stokes equations are solved, while realizing that the smaller scales cannot be resolved for high-Reynolds-number turbulent flows. Modeling is used to account for the effect of these unresolved scales on the resolved ones.

The objective of this work is to develop an LES code for studying ejector/mixer flow with an emphasis on capturing the flow and acoustic disturbances. In classical fan/duct noise, the noise source is computed separately and then matched to the duct modes.[8] But in the present approach, the simulation directly captures the source coupled with the duct modes. The governing equations are presented in Sec. II. Because of the wavelike nature of these disturbances, a high-order scheme is needed with low dispersion and dissipation errors. The dispersion-relation-preserving (DRP) scheme[9] is used herein, as outlined in Sec. III. High-order schemes can allow spurious modes to be introduced at the computational boundaries, which contaminate the physical solution. As such, special attention is given herein to unsteady boundary treatments, as outlined in Sec. IV. Simulation and discussion of the results are given in Sec. V.

II. Governing Equations

We consider herein the nozzle ejector flow shown in Fig. 2. The primary nozzle diameter is D, and its inlet mean flow velocity is u_j. The flow variables are nondimensionalized as follows: lengths by the primary nozzle diameter D, velocities by the primary jet velocity u_j, time by D/u_j, density by the jet inlet density ρ_j, and pressure by ρu_j^2. Starting from the full, time-dependent compressible Navier–Stokes equations, a spatial filter is introduced in the form

$$f(x) = \int_D K(x - z, \Delta) f(z)\, \mathrm{d}z \tag{1}$$

where K is the spatial filter function, Δ is the computational mesh size, and D is the flow domain. Upon applying this filter to the flow variables, the flowfield can be decomposed into

$$f = \bar{f} + f'' \tag{2}$$

where an overbar denotes the resolved (filtered) field and a $''$ denotes the unresolved (subgrid) one. The mean of the filtered field is the mean of the total field. Upon substituting this splitting into the full Navier–Stokes equations, the filtered compressible Navier–Stokes equations in cylindrical coordinates take the form[10–12]

$$\frac{\partial Q}{\partial t} + \frac{\partial F}{\partial x} + \frac{1}{r}\frac{\partial (rG)}{\partial r} + \frac{1}{r}\frac{\partial H}{\partial \chi} = S \tag{3}$$

$$Q = [\bar{\rho}, \bar{\rho}\bar{u}, \bar{\rho}\bar{v}, \bar{\rho}\bar{w}, \bar{\rho}\bar{e}]^T \tag{4}$$

$$F = \begin{bmatrix} \bar{\rho}\bar{u} \\ \bar{p} + \bar{\rho}\bar{u}^2 - \bar{\sigma}_{xx} - \upsilon_{xx} \\ \bar{\rho}\bar{u}\bar{v} - \bar{\sigma}_{xr} - \upsilon_{xr} \\ \bar{\rho}\bar{u}\bar{w} - \bar{\sigma}_{x\chi} - \upsilon_{x\chi} \\ \bar{\rho}\bar{u}\bar{I} - \bar{u}\bar{\sigma}_{xx} - \bar{v}\bar{\sigma}_{xr} - \bar{w}\bar{\sigma}_{r\chi} - \bar{\kappa}\dfrac{\partial \bar{T}}{\partial x} - c_v q \end{bmatrix} \tag{5}$$

$$G = \begin{bmatrix} \bar{\rho}\bar{v} \\ \bar{\rho}\bar{u}\bar{v} - \bar{\sigma}_{xr} - \upsilon_{xr} \\ \bar{p} + \bar{\rho}\bar{v}^2 - \bar{\sigma}_{rr} - \upsilon_{rr} \\ \bar{\rho}\bar{v}\bar{w} - \bar{\sigma}_{r\chi} - \upsilon_{r\chi} \\ \bar{\rho}\bar{v}\bar{I} - \bar{u}\bar{\sigma}_{xr} - \bar{v}\bar{\sigma}_{rr} - \bar{w}\bar{\sigma}_{r\chi} - \bar{\kappa}\dfrac{\partial \bar{T}}{\partial r} - c_v q \end{bmatrix} \tag{6}$$

Presented as Paper 96-1731 at the AIAA/CEAS 2nd Aeroacoustics Conference, State College, PA, 6–8 May 1996; received 12 July 1997; revision received 14 April 1998; accepted for publication 14 April 1998.

*NRC Fellow. Member AIAA.
†Technical Leader; fsmankb@lerc.nasa.gov.

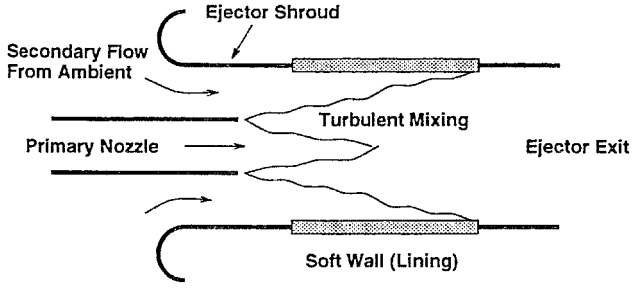

Fig. 1 Ejector with single-element primary nozzle.

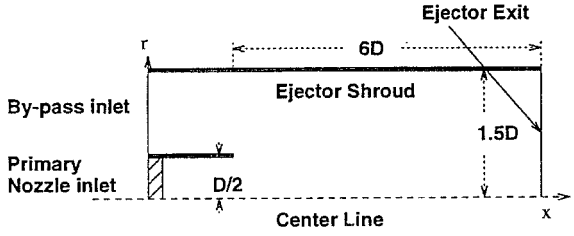

Fig. 2 Computation domain.

$$H = \begin{bmatrix} \bar{\rho}\bar{w} \\ \bar{\rho}\bar{u}\bar{w} - \bar{\sigma}_{x\chi} - \upsilon_{x\chi} \\ \bar{\rho}\bar{v}\bar{w} - \bar{\sigma}_{r\chi} - \upsilon_{r\chi} \\ \bar{p} + \bar{\rho}\bar{w}^2 - \bar{\sigma}_{\chi\chi} - \upsilon_{\chi\chi} \\ \bar{\rho}\bar{w}\bar{I} - \bar{u}\bar{\sigma}_{x\chi} - \bar{v}\bar{\sigma}_{r\chi} - \bar{w}\bar{\sigma}_{\chi\chi} - \bar{\kappa}\dfrac{\partial \bar{T}}{\partial \chi} - c_v q \end{bmatrix} \tag{7}$$

$$S = \frac{1}{r}\begin{bmatrix} 0 \\ 0 \\ \bar{p} + \bar{\rho}\bar{w}^2 - \bar{\sigma}_{\chi\chi} - \upsilon_{\chi\chi} \\ -\bar{v}\bar{w} - \bar{\sigma}_{r\chi} - \upsilon_{r\chi} \\ 0 \end{bmatrix} \tag{8}$$

Here, Q is the unknown vector; F, G, and H are the fluxes in the axial direction x, the radial direction r, and the azimuthal direction χ, respectively; S is the source term that arises in cylindrical polar coordinates; and κ is thermal conductivity. The enthalpy is I, the internal energy is e, and σ_{ij} is the viscous stresses. This system of equations is coupled with the equation of state for a perfect gas. Here, a tilde denotes Favre averaging

$$\tilde{f} = \overline{\rho f}/\bar{\rho} \tag{9}$$

The unresolved stresses, υ_{ij}, appearing in Eqs. (4–7) need to be modeled. Smagorinsky's model[13] is used for this purpose. In this model the subgrid-turbulence stresses are modeled as

$$\upsilon_{ij} = k_g \delta_{ij}/3 - 2\rho v_R\left(\bar{S}_{ij} - \tfrac{1}{3}\delta_{ij}\bar{S}_{mm}\right) \tag{10}$$

where k_g is the kinetic energy of the residual turbulence. The strain rate of the resolved scale is given by

$$\bar{S}_{ij} = \frac{1}{2}\left(\frac{\partial \bar{u}_i}{\partial x_j} + \frac{\partial \bar{u}_j}{\partial x_i}\right) \tag{11}$$

The summation $\bar{S}_{mm}$ is zero for incompressible flow, v_R is the effective viscosity of the residual field

$$v_R = (C_s \Delta_f)^2\sqrt{2S_{mn}S_{mn}} \tag{12}$$

and Δ_f is the filter width given by

$$\Delta_f = (\Delta_x \Delta_r \Delta_\chi)^{\frac{1}{3}} \tag{13}$$

For the heat equation Edison[14] proposed the eddy viscosity model

$$q = \bar{\rho}\frac{v_t}{Pr_t}\frac{\partial \tilde{T}}{\partial x_k} \tag{14}$$

where Pr_t is the subgrid-scale turbulent Prandtl number, which is taken as 1.0, and $C_S = 0.1$.

III. Numerical Discretization

The DRP scheme of Tam and Webb[9] is used herein with selective artificial damping. The governing equations are written as

$$Q_{l,m}^{(n+1)} = Q_{l,m}^{(n)} + \Delta t\sum_{j=0}^{3} b_j K_{l,m}^{(n-j)} \tag{15}$$

where

$$K_{l,m}^{(n)} = -\frac{1}{\Delta x}\sum_{j=-3}^{3} a_{i+j,m}^{(n)} - \frac{1}{\Delta r}\sum_{j=-3}^{3} a_j G_{l,m+j}^{(n)} - \frac{1}{r_m}G_{l,m}^{(n)}$$

$$+ S_{l,m}^{(n)} - \frac{\mu_a}{(\Delta r)^2}\sum_{j=-3}^{j=3} d_j Q_{l+j,m}^{(n)} - \frac{\mu_a}{(\Delta r)^2}\sum_{j=-3}^{3} d_j Q_{l,m+j}^{(n)} \tag{16}$$

The coefficients appearing in Eqs. (15) and (16) are given in Refs. 9 and 15.

IV. Boundary Conditions

A. Wall Boundary Conditions

On the solid surfaces of the primary nozzle and ejector, the slip boundary condition is applied. No-slip requires additional fine grid points to resolve the viscous layer. This will allow the formation of Goetler vortices and Tollmien–Schlichtung waves. One of the objectives herein is to introduce a solid wall treatment that prevents the generation of spurious modes. Implementing the slip condition allows testing such treatment without additional modes generated by wall viscous effects, and eliminates the need for more grid points.

To maintain the accuracy of the scheme, the minimum-ghost-points approach of Tam and Dong[15] is adopted. Bias interior differencing is used to avoid introducing unnecessary ghost points. The coefficients of the interior differencing are derived in a way consistent with the interior DRP scheme.

B. Outflow Boundary Conditions

The crossing of flow and acoustics disturbances at the outflow boundary could produce artificial reflections that contaminate the physical solution. Tam and Webb's[9] asymptotic outflow treatment has proven to be quite successful in jet noise simulation. However, in the jet simulation case,[6,16] the computational domain is long enough such that the mean flow gradient is weak and both the vorticity and acoustic modes are important at the outflow. But, in the present computation, the mean flow gradient at the outflow boundary is significant. The mean flow profile is of inflection-type profile suggesting the formation of strong Kelvin–Helmholtz instability waves. Assuming the dominance of convected instability waves at the outflow boundary, Tam[17] proposed the following outflow treatment:

$$\left(\frac{\partial}{\partial t} + C_0\frac{\partial}{\partial x} - C_1\frac{\partial^3}{\partial x^3}\right)[\hat{\rho}, \hat{u}, \hat{v}, \hat{p}] = 0 \tag{17}$$

where the circumflex denotes the fluctuating quantities. The constants C_0 and C_1 are obtained from the dispersion relation of the instability waves. In the present computation only the first-order derivative term is used, where C_0 is the phase speed of the instability wave.

Because of nonlinear effects, various frequency modes will be present at downstream locations, even if the initial disturbance is characterized by a single frequency. The critical-layer theory[18,19] suggests that modes generated by interaction will be harmonics and

subharmonics of phase velocities close to the fundamental one. For a mixing layer formed by two streams of velocities u_1 and u_2 ($u_1 > u_2$), c_0 is approximately taken as $C_0 = u_2 + 0.7(u_1 - u_2)$, which is a good estimate for the phase velocities for frequencies at a Strouhal number less than 1.0 (Ref. 20).

C. Inflow Boundary Conditions

At the primary nozzle the flow is supersonic and flow variables are given as

$$[\rho, u, v, p] = [\rho_j, u_j, 0, p_j]$$

$$+ \varepsilon Re[\hat{\rho}(kr), \hat{u}(kr), \hat{v}(kr), \hat{p}(kr)] \exp[i(kx - \omega t)] \qquad (18)$$

The first term in the right-hand side of Eq. (18) is the mean flow, whereas the second term is the disturbance source of amplitude ε. The radial distribution of the source is given as the eigenfunctions of the duct modes in the radial direction, which are composed of Bessel functions. For a given frequency, k is the corresponding wave number, which is given[21] as

$$k/\omega = 1/\left(M_j^2 - 1\right)\left[M_j \pm \sqrt{1 + \left(M_j^2 - 1\right)(k/\omega)}\right] \qquad (19)$$

where M_j is the primary flow Mach number.

At the inlet of the bypass channel the flow is subsonic and the first-order absorbing boundary condition of Engquist and Majda[22] is used. Namely,

$$\frac{\partial}{\partial t}[\rho, u, v, p] + (\bar{u} - \bar{c})\frac{\partial}{\partial x}[\hat{\rho}, \hat{u}, \hat{v}, \hat{p}] = 0 \qquad (20)$$

where c is the speed of sound.

V. Simulations and Results

Figure 2 shows the geometry for the present simulations. The diameter of the ejector shroud is taken as three dimensional, where D is the diameter of the primary nozzle. The nozzle length is one dimensional and that of the shroud is six dimensional. The total temperature is constant over the computational domain. At the start of the computation, the mean flow at the inlet is uniform with the Mach number for the primary nozzle $M_j = 1.5$, whereas that of the coflow is $M_b = 0.4$. The static pressure is uniform at the inlet. The Reynolds number based on the primary nozzle diameter is 1×10^3 and the Prandtl number is 0.72. The initial disturbance is taken to be of single frequency corresponding to a Strouhal number of $St = 0.2$, where $St = fD/u_j$, f is the frequency in Hz $= \omega/2\pi$. In the disturbance source [Eq. (18)], only the first duct mode in the r direction is considered, corresponding to uniform distribution in r. The amplitude level is taken $\varepsilon = 0.025$.

Regarding grid sizing, the objective here is to accurately capture the unsteady disturbance field, which is composed of various frequencies and wavelengths. Several studies on grid resolution using the DRP scheme for this configuration and for other configurations were performed.[23–25] The grid convergence was found to depend on the wavelength considered. With the DRP scheme six grid points per wavelength were necessary to achieve grid independence. The mesh size was chosen here to be $\Delta x = \Delta r = D/33$. With these parameters, the largest Strouhal number that can be captured accurately herein is $St = 4$. Higher Strouhal number waves are considered unresolved and are accounted for by the subgrid model.

The dimensionless ratio $\Delta t/\Delta x$ is 0.0125, to ensure stability and low numerical dispersion. The dimensionless artificial viscosity in Eq. (16) is taken $\mu_a = 6 \times 10^{-3}$ to suppress the high-frequency spurious modes. This choice of μ_a has a very small effect on the acoustic waves with a wavelength longer than $6\Delta x$, as indicated in Ref. 15.

The simulation is carried out on IBM RS/6000 workstations. After the transients have left the computational domain, a periodic stage of period T is reached. The solution continues until no-cycle-to-cycle variation is reached. The mean flow solution is then computed by averaging the solution over the last two periods. The process takes about 8 CPU hours with almost three-quarters of the time for the transients to leave the computational domain.

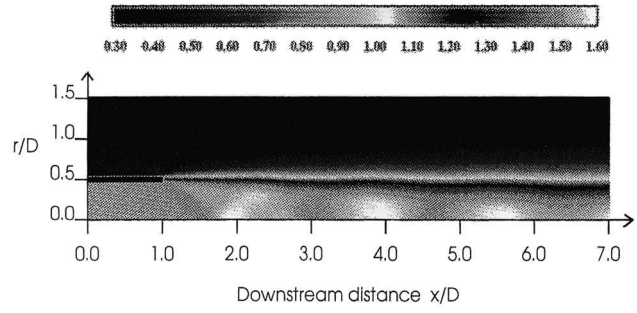

Fig. 3 Mach number distribution of the mean flow.

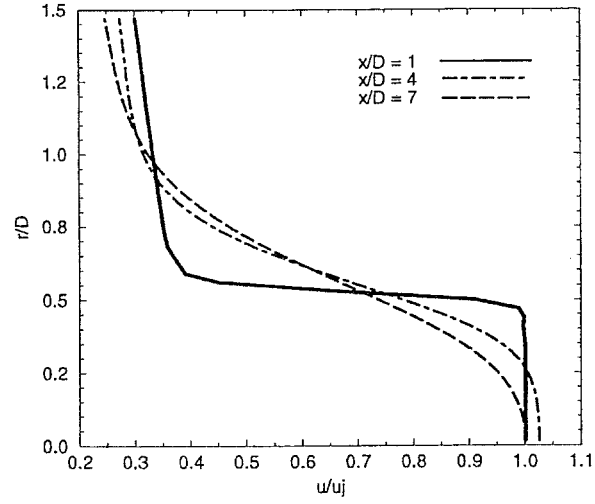

Fig. 4 u-velocity profiles at various downstream locations.

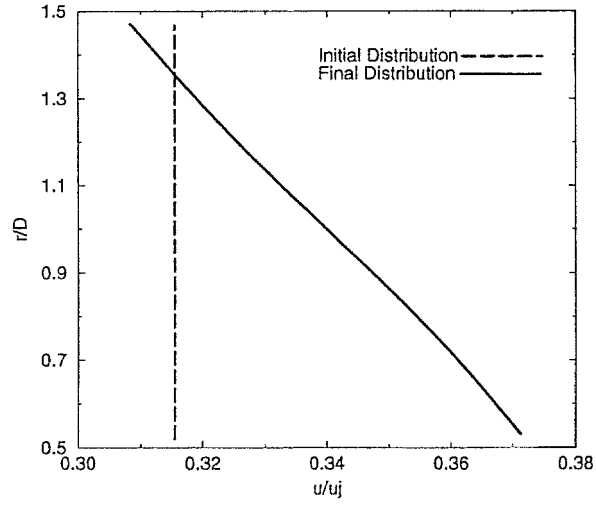

Fig. 5 u-velocity across the inlet boundary of the bypass channel.

The mean Mach number distribution is shown in Fig. 3. As expected, a shear layer is formed because of the velocity difference between the inner and outer stream. The shear layer starts from the trailing edge of the nozzle and grows in the downstream direction. The mixing and growth of the shear layer is also depicted in Fig. 4, which shows the mean flow profile at various axial locations. The nearly top-hat profile is modified to a smoother profile in the downstream direction. One of the major issues in numerical simulation of jet flow is to account for the entrainment effect. In Fig. 5, the mean flow profile at the trailing-edge point is magnified. We note that, while the initial distribution is assumed to be uniform, the final

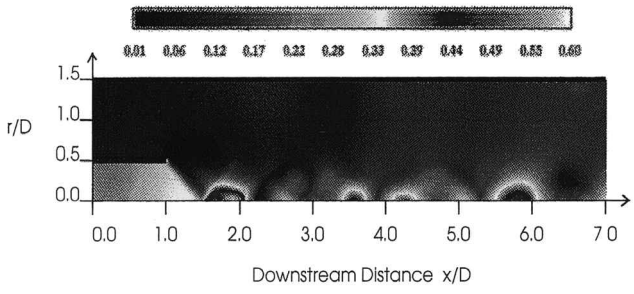

Fig. 6 Root mean square of pressure fluctuations.

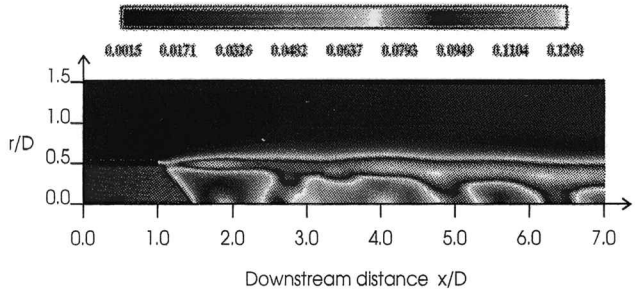

Fig. 7 Root mean square of axial momentum fluctuation.

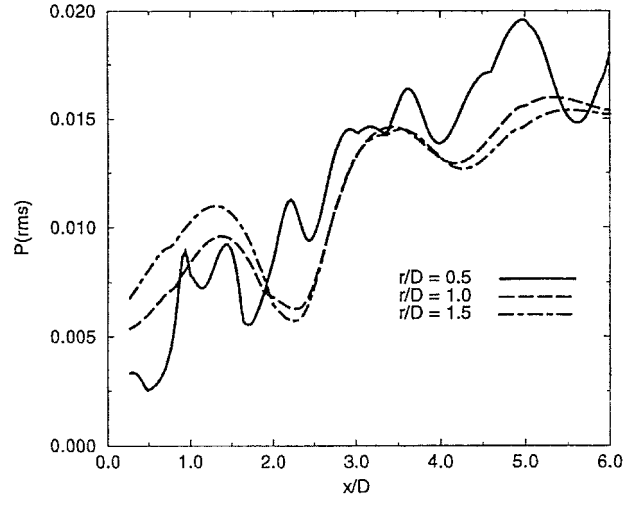

Fig. 8 Root mean square of pressure fluctuations at various radial locations.

solution exhibits entrainment of the mean flow, which is particularly pronounced near the surface of the separation plate.

The rms of the pressure and momentum fluctuations is shown in Figs. 6 and 7. In Fig. 8 the axial distribution of the rms of the pressure fluctuations for several radii is shown. Examining Fig. 3, 6–8 indicates that two structures can be identified. The first is the usual large-scale structure,[26,27] which is wavelike. This structure grows in the downstream direction and resembles nonlinear instability waves interacting with the mean flow and the small-scale turbulence. In addition to this structure, a weak shock-cell structure can be identified. This can be attributed to the formation of weak shock waves and expansion waves. The simulation is set for a perfectly expanded inner jet. But, because of the unsteady fluctuations, the inner jet actually switches in time, between an overexpanded and underexpanded jet. This leads to the formation of alternating expansion and shock waves, which interacts with the large-scale structure and forms the weak shock-cell structure, and the wiggles in the streamwise development of the pressure's rms.

The power spectrum of the axial velocity at the shear-layer lip ($r/D = 0.5$), computed at various downstream locations, is plotted in Fig. 9. The spectrum is obtained by taking discrete Fourier transform of the time derivative of u. Therefore, the mean is automatically dropped out. The disturbance is initially composed of a single frequency corresponding to $St = 0.2$. However, nonlinear interaction causes the generation of other modes. By $x/D = 6$, the first harmonic ($St = 0.4$) becomes of comparable magnitude to that of the fundamental.

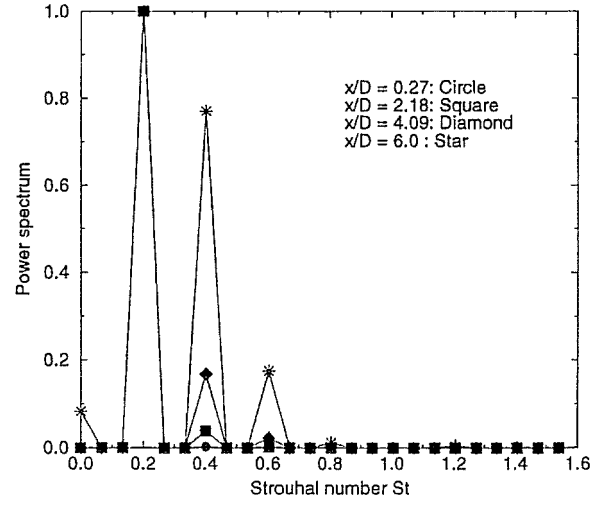

Fig. 9 Power spectrum of axial velocity at various downstream locations in the mixing layer $r/D = 0.5$.

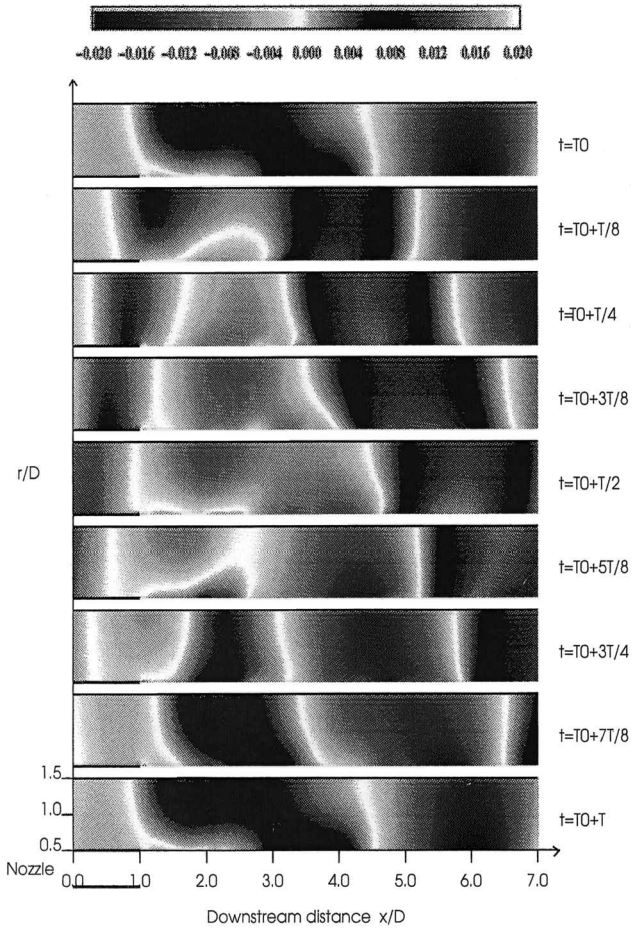

Fig. 10 Instantaneous pressure fluctuations at nine stages of the period T in the region above the shear layer ($r/D > 0.5$).

Figure 10 shows snapshots of the pressure fluctuations at nine stages of a period in the region $r/D > 0.5$. The change of color

along the line $r/D = 0.5$ indicates a wavelike structure that resembles Kelvin–Helmholtz instability waves. Starting from the top part of the figure and moving down shows that this large-scale structure is convected by the flow in the downstream direction. The figure also shows that a wavelike structure moves in the upstream direction opposite to the direction of flow. Both the upstream and downstream-convected structure is influenced by the presence of the top wall, indicating coupling with duct modes. As the convected structure moves away from the trailing edge, a normal front is formed corresponding to the plane duct mode. No noticeable reflection from the ejector exit or from the bypass channel inlet are observed in Fig. 10. This indicates the accuracy of the boundary condition used herein.

In supersonic mixing layers it is believed that the noise is dominated by radiation from a supersonically convected instability wavelike structure. For a given Strouhal number, the structure captured herein is wavelike, but, because of flowdivergence effects, it is not exactly harmonic in X. It can be viewed as being composed of various streamwise Fourier components. Thus, for a given frequency, there are several streamwise-Fourier components with various streamwise wavelengths. Some of these components are of supersonic wave speeds, even if the flow is subsonic. Thus, a large-scale structure in subsonic, diverging shear layers can produce sound.

VI. Conclusions

Numerical simulation of mixing inside an ejector/nozzle configuration is performed. The emphasis is on capturing the time-dependent flow and acoustic disturbances. The DRP scheme is used with proper boundary treatments at inflow, outflow, and solid walls to capture the physical disturbances while eliminating the spurious ones. Results show that a spatially growing mixing layer is formed starting at the separation point. Because of the mean flow gradient, the disturbances grow in amplitude. Plane wave fronts are formed and propagate in the upstream and downstream directions, and can leave the outflow and inflow boundaries without artificial reflections. While the simulation is for a nominally perfectly expanded inner jet, a weak shock-cell structure can be detected. This is attributed to the fluctuating nature of the disturbances, which cause alternating weak shock or expansion waves. The disturbances are initially composed of a single frequency. But, because of the nonlinearity, other harmonics and subharmonics are generated and grow to fill the spectrum.

Acknowledgment

This work was performed while the first author held a National Research Council Associateship.

References

[1]Lord, W. K., Jones, C. W., Head, V. L., and Krejsa, E. A., "Mixer Ejector Nozzle for Jet Noise Suppression," AIAA Paper 90-1909, July 1995.

[2]Tillman, T. G., Paterson, R. W., and Presz, W. M., "Supersonic Nozzle Mixer Ejector," *Journal of Propulsion and Power*, Vol. 8, No. 2, 1992, pp. 513–519.

[3]Jones, R. R., III, Ahuja, K. K., Tam, C. K. W., and Abdelwahab, M., "Measured Acoustic Characteristics of Ducted Supersonic Jets at Different Model Scales," AIAA Paper 93-0731, 1993.

[4]Ahuja, K. K., Massey, K. C., and Entrekin, A. C., "Contribution of Mixing Within an Ejector to the Farfield Noise Measurements," AIAA Paper 96-0639, 1996.

[5]Mankbadi, R. R., Hayder, M. E., and Povinelli, L. A., "Structure of Supersonic Jet Flow and Its Radiated Sound," *AIAA Journal,* Vol. 32, No. 5, 1994, pp. 897–906.

[6]Mankbadi, R. R., Shih, S. H., Hixon, R., and Povinelli, L. A., "Direct Computation of Sound Radiation by Jet Flow Using Large-Scale Equations," AIAA Paper 95-0680, Jan. 1995.

[7]Morris, P. J., Wang, Q., Long, L. N., and Lockard, D. P., "Numerical Predictions of High Speed Jet Noise," AIAA Paper 97-1598, 1997.

[8]Huff, D. L., "Fan Noise Prediction: Status and Needs," AIAA Paper 98-0177, 1998.

[9]Tam, C. K. W., and Webb, J. C., "Dispersion-Relation-Preserving Finite-Difference Schemes for Computational Aeroacoustics," *Journal of Computational Physics*, Vol. 107, Aug. 1993, pp. 262–281.

[10]Erlebacher, G., Husaini, M. Y., and Speziale, C. G., "Toward the Large-Eddy Simulation of Compressible Turbulent Flows," *Journal of Fluid Mechanics*, Vol. 238, 1992, pp. 155–185.

[11]Zang, T. A., Dahlburg, R. B., and Dahlburg, J. P., "Direct and Large-Eddy Simulations of Three-Dimensional Compressible Navier–Stokes Turbulence," *Physics of Fluids A*, Vol. 4, No. 1, 1992, pp. 127–140.

[12]Mankbadi, R. R., *Transition, Turbulence, and Noise*, Kluwer, Dordrecht, The Netherlands, 1994.

[13]Smagorinsky, J., "General Circulation Experiments with the Primitive Equations, I. The Basic Experiment," *Monthly Weather Review*, Vol. 91, 1963, pp. 99–164.

[14]Edison, T. M., "Numerical Simulation of Turbulent Rayleigh-Bernard Problem Using Numerical Subgrid Modeling," *Journal of Fluid Mechanics*, Vol. 158, 1985, pp. 245–268.

[15]Tam, C. K. W., and Dong, T. Z., "Wall Boundary Conditions for High-Order Finite Difference Schemes in Computational Aeroacoustics," *Theoretical and Computational Fluid Dynamics*, Vol. 6, 1994, pp. 303–322.

[16]Mankbadi, R. R., Hixon, D. R., Shih, S.-H., and Povinelli, L. A., "Linearized Euler Equations as a Tool in Jet Noise Prediction," *AIAA Journal*, Vol. 36, No. 2, 1998, pp. 140–147.

[17]Tam, C. K. W., "Outflow Boundary Conditions for Instability and Dispersive Waves" (in preparation).

[18]Craik, A. D. D., "Resonant Interactions in Shear Flows, *Laminar-Turbulent Transition*, edited by V. V. Kozlov, Springer–Verlag, New York, 1986, pp. 1–8.

[19]Mankbadi, R. R., Wu, X., and Lee, S. S., "A Critical Layer Analysis of the Resonant Triad in Boundary-Layer Transition: Nonlinear Interactions," *Journal of Fluid Mechanics*, Vol. 256, 1993, pp. 85–106.

[20]Michalke, A., "Instabilitat eins Kompressiblen rundem Freistahls inyer eruck-sichtingung des Einflusses der Strahlgrenzschichtdicke," *Zeitschrift filr Flugwissenschaften*, Vol. 19, 1971, p. 317.

[21]Eversman, W., "Theoretical Models for Duct Acoustic Propagation and Radiation," NASA RP 1258, Vol. 2, 101, 1991.

[22]Engquist, B., and Majda, A., "Absorbing Boundary Conditions for the Numerical Simulation of Waves," *Mathematics of Computations*, Vol. 31, July 1977, pp. 629–651.

[23]Dong, T. Z., and Mankbadi, R. R., "Numerical Simulations of Small Amplitude Acoustic Wave Propagation in a Converging-Diverging Nozzle," *Proceedings of the ICASE/LaRC Workshop on Computational Aero-Acoustics*, Inst. for Computer Applications in Science and Engineering, Hampton, VA, 1995, pp. 285–290.

[24]Dong, T. Z., and Mankbadi, R. R., "Direct Numerical Simulations of Engine Internal Noise Propagation and Radiation," AIAA/CEAS Paper 95-064, June 1995.

[25]Dong, T. Z., Shih, S. H., Mankbadi, R. R., and Povinelli, L. A., "A Numerical Study of Duct Geometry Effect on Radiation of Engine Internal Noise," AIAA Paper 97-16-4, May 1997.

[26]Liu, J. T. C., "Contribution to the Understanding of Large-Scale Coherent Structures in Developing Free Turbulent Shear Flows," *Advances in Applied Mechanics*, Vol. 26, 1988, pp. 183–309.

[27]Liu, J. T. C., "Coherent Structure in Transitional and Turbulent Shear Flows," *Annual Review of Fluid Mechanics*, Vol. 21, 1989, pp. 285–315.